From amplification of spontaneous emission to saturation in x-ray lasers: A Maxwell-Bloch treatment

Alain Sureau and Philip B. Holden
Laboratoire de Spectroscopie Atomique et Ionique, URA 775 du CNRS, Université Paris-Sud, Bâtiment 350, F-91405 Orsay, Cedex, France
(Received 20 January 1995; revised manuscript received 1 June 1995)

The interaction between radiation and matter in an x-ray laser occurring in a cylindrical laser-produced plasma is investigated by means of the Maxwell-Bloch equations with level degeneracies explicitly taken into account. Radiation is initiated by spontaneous emission and amplified while propagating along the cylinder axis. This theory generalizes the current simple theory of the small-signal gain coefficient and is suited to correctly describe the gradual transition to the saturation regime. A detailed numerical study of the germanium x-ray laser is performed to illustrate the theory for the case of the Ne-like ion collisional laser. The effect of electron-ion collisions leading to transitions between degenerate states on linewidths, as well as on saturation behavior is outlined.

PACS number(s): 42.55.Vc, 32.80.Bx

I. INTRODUCTION

In x-ray laser studies [1] the theory of amplification of spontaneous emission (ASE) with a (constant) small-signal gain coefficient fails to describe the evolution of the radiation when the intensity becomes large. This problem is generally overcome by the use of the steady-state saturation intensity [2–4] which enables the effect of stimulated transitions on the populations to be modeled indirectly. This treatment, however, fails to directly model changes in the level populations (potentially significant in a system which has several lasing transitions which may be coupled) and, more importantly, neglects to model certain quantum-mechanical effects which arise in a linearly propagating field. It is possible to overcome both of these limitations by combining the Maxwell wave equation and the Bloch equations (which govern the time evolution of the density-matrix elements), taking into account the electric-dipole interaction between the radiation and the ions of the plasma constituting the amplifying medium. The population rate equations must, of course, additionally include all the other mechanisms (spontaneous radiative decay, collisional excitations and de-excitations, ionization and recombination) which populate or depopulate the individual states. A number of works have already used the Maxwell-Bloch equations as the basis for specific investigations such as the buildup of radiation [5], gain [6], transverse coherence [7,8], superfluorescence [9], and superradiance [10] theory. However, in x-ray laser studies, apart from purely theoretical preliminary works [11], the degenerate atomic structure of the ionic levels has not yet been specifically considered for the numerical treatment of the interaction of the ASE electric field with the medium.

In the present work, the level degeneracies have been explicitly taken into account to derive the Maxwell-Bloch equations which self-consistently govern the evolution of the population of the plasma ionic states and the evolution of the (unpolarized) spontaneous emission which is amplified while propagating through the active medium. The population inversions themselves depend upon the intensity of the radiation through the population rate equations. The customary paraxial approximation (see, for example, Ref. [5]) is used to manage the Maxwell wave equation, and coherences of the density matrix are assumed to be in the steady state with respect to their production and decay processes. The wave equation so obtained contains a real part and an imaginary part which can be separately analyzed.

The real part gives the spatial evolution of the phase of the wave electric field as a function of the free-electron density and of the population inversions. The refractive index of the medium for the wave can then be determined.

The imaginary part gives the spatial evolution of the amplitude of the electric field as a function of the population inversion. The (local intensity) gain coefficient can be then deduced directly and is expressed in a form which reduces to the small-signal gain coefficient at low intensity. The gain value is consistent with the Einstein coefficient of stimulated emission as calculated by the Fermi golden rule.

At high intensities the population of each interacting energy level (αJ)—where α stands for specifications (electronic configuration and so on) and J for total angular-momentum quantum number of the level—can no longer be considered as an entity to which a rate coefficient of stimulated emission (or absorption) is associated. As a consequence of the nature of linearly propagating radiation— all electric-field oscillations occur in the plane perpendicular to the direction of propagation—the interaction between the radiation and each individual state (αJM) is, in general, different for each state and must be taken into account, as shown in this work. The elastic electron-ion collisions of the type $(\alpha JM)+e^- \rightarrow (\alpha JM')+e^-$ must also be considered, as these tend to restore equilibrium populations among the states of a same level. The present theory is appropriate

to describe the gradual transition from ASE to saturation.

This paper presents first, in Sec. II, a résumé of the simple ASE regime, valid for low intensity with the small-signal gain coefficient. This is presented for comparison with the results of a more elaborate theory derived in subsequent parts. In Sec. III, the basic equations leading to the Maxwell-Bloch equations are given in their complete generality. Section IV develops the problem with approximations for practical applications. Section V is devoted to the refractive index of the medium and Sec. VI to the gain, intensity, and population evolutions. It is shown in Sec. VII that the simple theory of Sec. II appears as the low-intensity approximation of the Maxwell-Bloch treatment, as expected. In Sec. VIII the particular case of the Ne-like collisional x-ray laser is presented in detail and a numerical study of saturation in a germanium plasma is performed. The conclusions are given in Sec. IX.

II. ASE REGIME WITH CONSTANT GAIN ALONG THE Z AXIS

The geometry of the problem is presented in Fig. 1. A plasma column (along the z axis) exhibits a population inversion between an upper level (u) and a lower level (l) which have population densities N_u and N_l, respectively. These levels are connected by an electric-dipole transition.

The intensity $I(\nu)$ of radiation at frequency ν of the associated spectral line with normalized profile $\Phi(\nu)$, propagating along increasing z satisfies

$$\frac{\partial I(\nu,z)}{\partial z}=j(\nu)+G(\nu)I(\nu,z) , \tag{1}$$

where $j(\nu)=N_u\{[A_{ul}\Phi(\nu)\Theta]/(4\pi)\}h\nu$ is the emissivity; $G(\nu)=\{[h\nu\Phi(\nu)]/c\}g_uB_{ul}\Delta n_{ul}$ is the gain; A_{ul} is the Einstein coefficient of spontaneous emission, $A_{ul}=[(8\pi h\nu^3)/(c^3)]B_{ul}$; B_{ul} is the Einstein coefficient of stimulated emission; $B_{ul}=[d^2/(6\hbar^2\varepsilon_0 g_u)]$, with $d=\langle u\|\vec{d}\|l\rangle$ and $\vec{d}$ the atomic dipole; g is the level statistical weight; Θ is the solid angle of emission; and $\Delta n_{ul}=N_u/g_u-N_l/g_l$ is the inversion density.

As long as $j(\nu)$ and $G(\nu)$ can be considered independent of z, the integration of Eq. (1) yields

$$I(\nu,z)=\frac{j(\nu)}{G(\nu)}(e^{G(\nu)z}-1)+I(\nu,0)e^{G(\nu)z} ,$$

i.e.,

$$I(\nu,z)=\frac{j(\nu)}{G(\nu)}(e^{G(\nu)z}-1) . \tag{2}$$

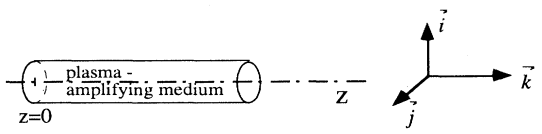

FIG. 1. Geometry of the problem.

It is useful to note that the ratio $\{[j(\nu)]/[G(\nu)I(\nu,z)]\}=[1/(e^{G(\nu)z}-1)]$ is only 10^{-2} when the product $G(\nu)z$ is as small as 4.6, which is far below saturation. So the first term on the right-hand side of Eq. (1) (the contribution of local spontaneous emission) is negligible with respect to the second term (the stimulated emission) for $G(\nu)z$ greater than 4.6 and Eq. (1) reduces to

$$\frac{\partial I(\nu,z)}{\partial z}=G(\nu)I(\nu,z) \quad [G(\nu)z\geq 4.6] . \tag{1'}$$

The populations are obtained from the population-rate equations

$$\frac{dN_i}{dt}=-N_i\Gamma_i+R_i , \tag{3}$$

where Γ_i is the total decay rate of level i and R_i is the sum of all processes populating the level i. In particular, Γ_u includes $A_{ul}+B_{ul}\int d\nu\{[I(\nu)]/c\}\Phi(\nu)$ and R_u includes $N_l[(g_uB_{ul})/g_l]\int d\nu\{[I(\nu)]/c\}\Phi(\nu)$; Γ_l includes $[(g_uB_{ul})/g_l]\int d\nu\{[I(\nu)]/c\}\Phi(\nu)$ and R_l includes $N_uB_{ul}\int d\nu\{[I(\nu)]/c\}\Phi(\nu)$.

At high intensity (large gain lengths) the populations [and hence $j(\nu)$ and $G(\nu)$] are no longer independent of z and the differential equation (1) cannot be integrated into Eq. (2). In addition, the individual states pertaining to a common level do not interact in the same way with the radiation, and their populations may differ from one state to another. At high intensity, another theoretical basis is necessary.

III. BASIC EQUATIONS

The Maxwell wave equation for radiation through the (globally neutral) plasma ($\vec{\nabla}\cdot\vec{E}=0$) is

$$\vec{\nabla}^2\vec{E}-\frac{1}{c^2}\frac{\partial^2\vec{E}}{\partial t^2}-\frac{\omega_{pe}^2}{c^2}\vec{E}=\frac{1}{\varepsilon_0c^2}\frac{\partial^2\vec{P}}{\partial t^2} , \tag{4}$$

where $\vec{E}=\vec{E}(x,y,z,t)$ is the electric field, $\vec{P}=\vec{P}(x,y,z,t)$ the polarization vector, and $\omega_{pe}=[(N_eq^2)/(\varepsilon_0m_e)]^{1/2}$ the electron plasma frequency (N_e being the free-electron density).

An electric field of transverse waves propagating along the z axis cannot include any component of $\vec{k}$, i.e., π-polarized radiation. Transverse fields being real vectors, and since spontaneous emission is right- or left-circularly polarized with equal statistical probabilities, $\vec{E}$ can be expressed as an incoherent superposition of $\sigma+$ and $\sigma-$ electric fields with the same (real) amplitude E but different (real) phases φ. The right-circularly polarized field $\vec{E}_{\sigma+}$ will then be expressed as

$$\vec{E}_{\sigma+}=E\cos(\omega t-kz+\varphi_+)\vec{i}+E\sin(\omega t-kz+\varphi_+)\vec{j}$$

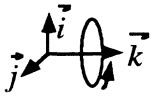

where $k=\omega/c$.

For standard tensorial components, the following spa-

tial unit vectors are introduced:[1]

$$\vec{e}_1=\frac{-\vec{i}+i\vec{j}}{\sqrt{2}},\quad \vec{e}_{-1}=\frac{\vec{i}+i\vec{j}}{\sqrt{2}},\quad \vec{e}_0=\vec{k}\ .$$

Setting $\tilde{E}=-E/\sqrt{2}$, this becomes

$$\vec{E}_{\sigma+}=\tilde{E}e^{i(\omega t-kz+\varphi_+)}\vec{e}_1-\tilde{E}e^{-i(\omega t-kz+\varphi_+)}\vec{e}_{-1}\ , \quad (5)$$

and similarly

$$\vec{E}_{\sigma-}=-\tilde{E}e^{-i(\omega t-kz+\varphi_-)}\vec{e}_1+\tilde{E}e^{i(\omega t-kz+\varphi_-)}\vec{e}_{-1}\ . \quad (6)$$

Corresponding emission and absorption processes are shown in Fig. 2.

The polarization vector $\vec{P}$ is given by

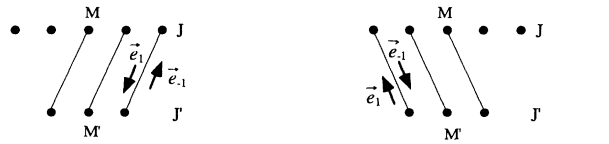

right-polarized wave σ+ left-polarized wave σ-

FIG. 2. The interaction of $\sigma+$ and $\sigma-$ radiation with a $J=2-J'=1$ transition.

$$\vec{P}=\mathrm{Tr}(\rho\vec{d})\ ,$$

where ρ is the density operator and $\vec{d}$ is the atomic electric dipole. It is shown in the Appendix that the equivalent useful expression is

$$\vec{P}=\sum_q\sum_M[\langle JM|d_q|J'M-q\rangle\rho_{J'M-q,JM}+(-1)^q\langle JM|d_{-q}|J'M+q\rangle\rho_{JM,J'M+q}]\vec{e}_q\ , \quad (7)$$

where $\rho_{JM,J'M'}=\langle JM|\rho|J'M'\rangle$.

We then consider the (Schrödinger) Bloch equation as

$$i\hbar\frac{\partial\rho}{\partial t}=[H,\rho] \quad (8)$$

with $H=H_A-\vec{d}\cdot\vec{E}$, where H_A is the atomic Hamiltonian with eigenstates $|JM\rangle$ such that

$$H_A|JM\rangle=W_J|JM\rangle\ ,$$

$$H_A|J'M'\rangle=W_{J'}|J'M'\rangle\ ,$$

$$W_J-W_{J'}=\hbar\omega_A\ .$$

The term $-\vec{d}\cdot\vec{E}$ describes the interaction between the radiation and the medium (dipolar approximation). As the density of emitters remains much smaller than λ^{-3} (λ being the wavelength of the radiation) dipole-dipole interactions are not considered [14]. The population density of any state is affected by a number of processes, notably free-electron collisions and possibly more than one radiative transition. The independent-rate approximation is used, i.e., the total evolution results from the sum of the different current processes. So, Eq. (8) determines the time evolution of the different ρ-matrix elements when completed by all other production and decay processes analogous to those occurring in Eq. (3). At $t=0$ the nondiagonal elements of ρ (coherences) are equal to zero and ρ may hence be written as

$$\rho=\sum_{JM}|JM\rangle\langle JM|n_{JM}\quad(t=0)\ ,$$

where $n_{JM}=\rho_{JM,JM}$ is the population density of the state JM.

IV. APPROXIMATIONS FOR PRACTICAL APPLICATIONS

Two main approximations are made.

(1) The energy nonconserving parts of the term $\vec{d}\cdot\vec{E}$ (atomic transition from a lower to an upper state with emission of one photon, or from an upper state to a lower state with absorption of one photon), which may occur if accompanied by a secondary process which serves to conserve energy, are ignored.

(2) The coherences (their envelopes) are assumed to be in quasi-steady state (QSS) with respect to their production and decay processes.

In the following, J and J' refer, respectively, to an upper and a lower level of a transition.

So, with $\Psi(\omega)$ defined by the relation

$$\frac{\Gamma-i\delta_L}{\delta_L^2+\Gamma^2}=\pi\Psi(\omega)\ , \quad (9)$$

so that $\int d\omega\,\Psi(\omega)=1$, where Γ is the collisional total decay rate of the coherences $\rho_{J'M',JM}$ (including the elastic electron-ion collisions), and $\delta_L=\omega-\omega_A$, one obtains (see the Appendix)

$$\vec{P}_{\sigma^+}=\frac{i\pi}{\hbar}\Psi(\omega)\sum_M\langle JM|d_1|J'M-1\rangle^2(n_{JM}-n_{J'M-1})\times\tilde{E}e^{i(\omega t-kz+\varphi_+)}\vec{e}_1+\mathrm{H.c.}\ . \quad (10)$$

$$\vec{P}_{\sigma^-}=\frac{i\pi}{\hbar}\Psi^*(\omega)\sum_M\langle JM|d_{-1}|J'M+1\rangle^2(n_{JM}-n_{J'M+1})\times\tilde{E}e^{-i(\omega t-kz+\varphi_-)}\vec{e}_1+\mathrm{H.c.} \quad (11)$$

[1]They are consistent with usual definitions of scalar product and vector product of complex vectors: $(A^{(1)}\cdot B^{(1)})=\sum_q(-1)^qA_qB_{-q}$ which, for Hermitian vectors, is equivalent to $\vec{A}\cdot\vec{B}^*$ (and $\vec{A}\cdot\vec{B}^*=\vec{A}^*\cdot\vec{B}$) and $\vec{A}\times\vec{B}=-i\sqrt{2}\{A^{(1)}B^{(1)}\}^{(1)}$, respectively (see Refs. [12,13]). The components of $\vec{A}=\sum_q A_q\vec{e}_q$ are given by $A_q=\vec{e}_q^*\cdot\vec{A}$. Then $A_x\vec{i}+A_y\vec{j}+A_z\vec{k}=A_1\vec{e}_1+A_{-1}\vec{e}_{-1}+A_0\vec{e}_0$ with $A_{\pm1}=\mp[(A_x\pm iA_y)/\sqrt{2}]$ and $A_0=A_z$.

It is worth noting that, within our approximations, only the coherences $\rho_{J'M-1,JM}$ and $\rho_{J'M+1,JM}$ are excited. Furthermore, the coherences $\rho_{J'M-1,JM}$ are excited only by $\sigma+$ fields and the coherences $\rho_{J'M+1,JM}$ only by $\sigma-$ fields.

It is shown in the Appendix that

$$\sum_M \langle JM|d_{-1}|J'M+1\rangle^2(n_{JM}-n_{J'M+1}) = \sum_M \langle JM|d_1|J'M-1\rangle^2(n_{JM}-n_{J'M-1}) .$$

For convenience we call $U_{JJ'}$ this common value:

$$U_{JJ'}=\sum_M \langle JM|d_{-1}|J'M+1\rangle^2(n_{JM}-n_{J'M+1}) = \sum_M \langle JM|d_1|J'M-1\rangle^2(n_{JM}-n_{J'M-1}) . \quad (12)$$

Therefore, with fields and polarizations given by Eqs. (5) and (10) for $\sigma+$ and Eqs. (6) and (11) for $\sigma-$, respectively, the usual paraxial approximation, and the retarded time variable $t-z/c$, Eq. (4) now becomes (see the Appendix)

$$\left[\frac{\partial\varphi}{\partial z}-\frac{\omega_{pe}^2}{2kc^2}\right]\tilde{E}-i\frac{\partial\tilde{E}}{\partial z}=-\frac{ikU_{JJ'}}{2\varepsilon_0\hbar}\pi\Psi(\omega)\tilde{E} ,$$

for $\sigma+$,

$$\left[\frac{\partial\varphi}{\partial z}-\frac{\omega_{pe}^2}{2kc^2}\right]\tilde{E}+i\frac{\partial\tilde{E}}{\partial z}=\frac{ikU_{JJ'}}{2\varepsilon_0\hbar}\pi\Psi^*(\omega)\tilde{E} ,$$

for $\sigma-$. These equations are the complex conjugates of one another.

Extracting the real part from each member we obtain *in both cases*

$$\frac{\partial\varphi}{\partial z}=\frac{\omega_{pe}^2}{2kc^2}-\frac{kU_{JJ'}}{4\varepsilon_0\hbar}\chi(\omega) , \quad (13)$$

where

$$\chi(\omega)=i\pi[\Psi(\omega)-\Psi^*(\omega)]=\frac{2\delta_L}{\delta_L^2+\Gamma^2}$$

and the imaginary part is

$$\frac{\partial\tilde{E}}{\partial z}=\frac{kU_{JJ'}}{4\varepsilon_0\hbar}\Phi(\omega)\tilde{E} \quad (14)$$

where

$$\Phi(\omega)=\pi[\Psi(\omega)+\Psi^*(\omega)]=\frac{2\Gamma}{\delta_L^2+\Gamma^2} .$$

V. REFRACTIVE INDEX

The refractive index of the medium for the radiation can be derived from Eq. (13). As long as $U_{JJ'}$ is independent of $\dot{z}$ (below saturation), one obtains

$$\varphi(z)=\varphi+\left[\frac{\omega_{pe}^2}{2kc^2}-\frac{kU_{JJ'}}{4\varepsilon_0\hbar}\chi(\omega)\right]z$$

and $\omega t-kz+\varphi(z)=\omega t-k'z+\varphi$ with

$$k'=k-\frac{\omega_{pe}^2}{2kc^2}+\frac{kU_{JJ'}}{4\varepsilon_0\hbar}\chi(\omega) .$$

Now the refractive index $n(\omega)$ is defined by $n(\omega)=k'/k$, i.e.,

$$n(\omega)=1-\frac{\omega_{pe}^2}{2\omega^2}+\frac{U_{JJ'}}{4\varepsilon_0\hbar}\chi(\omega) .$$

The refractive index at line center [$\chi(\omega_A)=0$] is

$$n(\omega_A)=1-\frac{\omega_{pe}^2}{2\omega_A^2}=1-\frac{1}{2}\frac{N_e}{N_c}=\left[1-\frac{N_e}{N_c}\right]^{1/2} ,$$

as often written, where $N_c=[(\varepsilon_0 m_e\omega_A^2)/(q^2)]$ is the critical density at ω_A (the relation $N_e\ll N_c$ is verified). It can be shown that, out of resonance ($\delta_L\neq 0$), the third term $[(U_{JJ'})/(4\varepsilon_0\hbar)]\chi(\omega)$ remains small (less than 1%) compared to the second term $\omega_{pe}^2/2\omega^2$ for cases of interest here.

VI. GAIN, INTENSITY, AND POPULATION EVOLUTIONS

The gain coefficient can be derived from Eq. (14). As

$$\int d\omega\,\Phi(\omega)=\int d\omega\,\pi[\Psi(\omega)+\Psi^*(\omega)]=2\pi$$

[see (9)], $\Phi(\omega)$ corresponds to $\Phi(\nu)$ such that

$$\int d\nu\,\Phi(\nu)=\frac{1}{2\pi}\int d\omega\,\Phi(\omega)=1 .$$

Then, using the variable ν instead of ω, Eq. (14) can be rewritten as

$$\frac{\partial\tilde{E}(\nu,z)}{\partial z}=\frac{kU_{JJ'}}{4\varepsilon_0\hbar}\Phi(\nu)\tilde{E}(\nu,z) , \quad (15)$$

where $\Phi(\nu)$ is the normalized line profile, as used in Eqs. (1) and (2). Furthermore, as the energy of the radiation propagating along a cylinder of section area S during the time interval T (volume cTS) is

$$\frac{\varepsilon_0}{2}\int d^3r(\vec{E}^2+c^2\vec{B}^2)=\varepsilon_0\int d^3r\,\vec{E}^2=\varepsilon_0 cTS\vec{E}^2 ,$$

the intensity on area S is $\varepsilon_0 c\vec{E}^2=2\varepsilon_0 c\tilde{E}^2(\nu,z)$ for both the $\sigma+$ and $\sigma-$ fields, and the total intensity when both fields are present is

$$I(\nu,z)=4\varepsilon_0 c\tilde{E}^2(\nu,z) .$$

Then

$$\frac{\partial I(\nu,z)}{\partial z}=\frac{kU_{JJ'}}{2\varepsilon_0\hbar}\Phi(\nu)I(\nu,z)$$

which may be written as

$$\frac{\partial I(\nu,z)}{\partial z}=G(\nu)I(\nu,z) \quad (16)$$

with

$$G(\nu)=\frac{k}{2\varepsilon_0\hbar}\Phi(\nu)\sum_M \langle JM|d_1|J'M-1\rangle^2(n_{JM}-n_{J'M-1}) \tag{17}$$

[see Eq. (12)]. Equation (16) is analogous to Eq. (1'). The expression (17) is a generalization of the quantity $G(\nu)$ used in relations (1), (1'), and (2) as shown in Sec. VII. The populations must be calculated with use of Eq. (8). Considering both the $\sigma+$ and $\sigma-$ fields, their contribution to $(d/dt)n_{JM}$ is

$$-[\langle JM|d_1|J'M-1\rangle^2(n_{JM}-n_{J'M-1})+\langle JM|d_{-1}|J'M+1\rangle^2(n_{JM}-n_{J'M+1})]\frac{\tilde{E}^2(\nu)\Phi(\nu)}{\hbar^2}$$

and their contribution to $(d/dt)n_{J'M}$ is

$$+[\langle JM+1|d_1|J'M\rangle^2(n_{JM+1}-n_{J'M})+\langle JM-1|d_{-1}|J'M\rangle^2(n_{JM-1}-n_{J'M})]\frac{\tilde{E}^2(\nu)\Phi(\nu)}{\hbar^2}\ .$$

Taking into account the whole line profile, the above relation between $I(\nu)$ and $\tilde{E}^2(\nu)$, and all other production and decay processes, we obtain finally

$$\begin{aligned}\frac{d}{dt}n_{JM}&=r_{JM}-\Gamma_{JM}n_{JM}-[\langle JM|d_1|J'M-1\rangle^2(n_{JM}-n_{J'M-1})\\&\quad+\langle JM|d_{-1}|J'M+1\rangle^2(n_{JM}-n_{J'M+1})]\int d\nu\frac{I(\nu)\Phi(\nu)}{4\hbar^2\varepsilon_0 c}\ ,\\\frac{d}{dt}n_{J'M}&=r_{J'M}-\Gamma_{J'M}n_{J'M}+[\langle JM+1|d_1|J'M\rangle^2(n_{JM+1}-n_{J'M})\\&\quad+\langle JM-1|d_{-1}|J'M\rangle^2(n_{JM-1}-n_{J'M})]\int d\nu\frac{I(\nu)\Phi(\nu)}{4\hbar^2\varepsilon_0 c}\ ,\end{aligned} \tag{18}$$

and the system is governed by Eqs. (16), (17), and (18).

Equation (18) determines the populations of the individual states and generalizes the equation system (3) which describes the populations of the energy levels. The r and Γ coefficients results from all populating and depopulating processes except those of absorption and stimulated emission associated with the radiation of the $J-J'$ transition, propagating along the z axis. Dealing with individual-state populations, elastic collisions (a transition occurring from one state to another state of the same energy level) must be taken into consideration. The corresponding rate dominates over other processes, and an estimation of the rate coefficient can be obtained from the formula [15]

$$\Gamma(s^{-1})\approx 3.87\times10^{-6}[N_e(\mathrm{cm}^{-3})]Z[T_e(\mathrm{eV})]^{-3/2}\ln\Lambda\ ,$$

where $\ln\Lambda$ is the Coulomb logarithm, and Γ is the frequency of electron-ion collisions with momentum transfer. In a neonlike selenium plasma ($Z=24$) with $N_e=3\times10^{20}$ cm^{-3} and $T_e=800$ eV, this gives $\Gamma\approx8\times10^{12}$ s^{-1}, and in a lithiumlike aluminum plasma ($Z=10$) with $N_e=10^{19}$ cm^{-3} and $T_e=30$ eV, this gives $\Gamma\approx9\times10^{12}$ s^{-1}, the same order of magnitude. Spontaneous-emission rates are generally much smaller. This is also true for absorption and stimulated emission rates and the lifetime of an ionic state is thus determined essentially by Γ which includes all inelastic and elastic electron-ion collisions. Spontaneous emission occurring from states of lifetime Γ^{-1} has the spectral profile of the Fourier transform of $e^{-\Gamma t}$, which is simply $\Phi(\omega)$. The normalized profile of the spontaneous emission is then given by $\Phi(\nu)$. Note that with $\Delta\lambda/\lambda=\Delta\omega/\omega=2\Gamma/\omega=\Gamma\lambda/\pi c$, i.e., $\Delta\lambda=\Gamma\lambda^2/\pi c$, one obtains $\Delta\lambda\approx40$ mÅ for $\lambda=200$ Å and $\Gamma=10^{13}$ s^{-1}. Such a situation occurs in a neonlike germanium plasma ($Z=22$) with temperatures and densities as considered in Sec. VIII. Total linewidths at $\lambda\approx200$ Å are estimated to be about 50 mÅ for this ion, while the Doppler width for ionic temperature $T_i=300$ eV is about 30 mÅ. The total width results from the Voigt profile obtained by convolution of the Lorentzian profile (collisional plus radiative decay, width about 40 mÅ) and the Gaussian profile (Doppler width about 30 mÅ), the resulting linewidth being smaller than the net addition of the two widths. It is to be noticed that the effect of electron-ion elastic collisions (with a transition from one state to another state of the same energy) on linewidths appears to be important. Different situations should be considered, according to different ΔM values, and states pertaining to different (more or less excited) levels. Specific quantitative values of the different rates of interest (not considered in the global formula of Ref. [15], and not available in general) would then be highly desirable.

As $I(\nu)$ is, in fact, z dependent according to (16), the populations [see (18)] and therefore the gain [see (17)] are themselves also z dependent. The set of equations [(16), (17), (18)] is locally valid and must be treated accordingly.

When the intensity $I(\nu)$ increases along the propagation axis, the linewidth full width at half maximum (FWHM) changes because the gain is frequency dependent. The line center being more amplified than the wings, the line shape is drawn out and thinned, resulting in the well-known effect of "gain narrowing." Labeling α the narrowing factor of the spectral line,

$\alpha=[(\Delta\nu)/(\Delta\nu_{\rm amp})]$ where $\Delta\nu$ is the linewidth (FWHM) of the profile $\Phi(\nu)$ and $\Delta\nu_{\rm amp}$ is the linewidth (FWHM) of the amplified radiation of intensity $I(\nu)$ at distance z, it is possible to show that, to good approximation, one may use

$$\int d\nu\, I(\nu)\Phi(\nu)=\frac{I(\nu_0)}{\alpha}$$

(ν_0 is the frequency at line center) and hence (18) can be written as

$$\frac{d}{dt}n_{JM}=r_{JM}-\Gamma_{JM}n_{JM}-\frac{I(\nu_0)}{4\alpha\hbar^2\varepsilon_0 c}[\langle JM|d_1|J'M-1\rangle^2(n_{JM}-n_{J'M-1})+\langle JM|d_{-1}|J'M+1\rangle^2(n_{JM}-n_{J'M+1})]\ ,$$
$$\frac{d}{dt}n_{J'M}=r_{J'M}-\Gamma_{J'M}n_{J'M}+\frac{I(\nu_0)}{4\alpha\hbar^2\varepsilon_0 c}[\langle JM+1|d_1|J'M\rangle^2(n_{JM+1}-n_{J'M})+\langle JM-1|d_{-1}|J'M\rangle^2(n_{JM-1}-n_{J'M})]\ . \tag{19}$$

As an illustration, we present in Sec. VIII an application with numerical codes, performed to study saturation in collisionally pumped Ne-like germanium x-ray lasers. We apply the theory to two lasing transitions which share a common lower level in the Ne-like ion, specifically the 196-Å and 236-Å transitions of Ge^{22+}.

VII. THE LOW-INTENSITY LIMIT

We show in this section that the simplified theory of Sec. II can be derived from Eqs. (16), (17), and (18) which govern the system. As long as the intensity is weak, stimulated emissions are negligible and the populations of the different states (JM) of one level J remain equal (any small deviation from equilibrium population is negated by elastic electron-ion collisions). In this case, $n_{JM}=n_J=N_J/(2J+1)$ where $N_J=\sum_M n_{JM}$. So, according to Eq. (17), $G(\nu)$ becomes

$$G(\nu)=\frac{k}{2\varepsilon_0\hbar}\Phi(\nu)(n_J-n_{J'})\sum_M\langle JM|d_1|J'M-1\rangle^2\ .$$

Owing to a sum rule of 3-j symbols the last sum is $d^2/3$, where $d=\langle J\|\vec{d}\|J'\rangle$. Then

$$G(\nu)=\frac{k}{2\varepsilon_0\hbar}\Phi(\nu)(n_J-n_{J'})\frac{d^2}{3}\ ,$$

or

$$G(\nu)=\frac{h\nu\Phi(\nu)}{c}g_J B_{JJ'}\Delta n_{JJ'}$$

as expected, and, from Eq. (18),

$$\frac{d}{dt}N_J=R_J-\Gamma_J N_J-(n_J-n_{J'})\frac{d^2}{6\hbar^2\varepsilon_0 c}\int d\nu\, I(\nu)\Phi(\nu)\ ,$$

or

$$\frac{d}{dt}N_J=R_J-\Gamma_J N_J-g_J(n_J-n_{J'})\frac{B_{JJ'}}{c}\int d\nu\, I(\nu)\Phi(\nu)$$

in agreement with the simplified theory of Sec. II.

VIII. NEONLIKE IONS, SATURATION IN GERMANIUM X-RAY LASERS

In recent years, the generation of high gain lengths and even saturation in Ne-like collisionally pumped x-ray lasers has become almost routine [16,3,17]. The method of theoretical investigation of such systems is generally through the use of a hydrodynamics and atomic physics package to generate a time-dependent description of the laser plasma which is post processed by either a ray-tracing [18,19] or a wave optics [20–23] treatment. The $2J+1$ degenerate states which comprise a laser level are assumed to react as a whole to the radiation field and the rate equations which describe the atomic populations concern the level populations and not specifically those of the degenerate states. Within such approximations, the role of saturation in determining the intensity of the laser output and a description of gain narrowing for arbitrary homogeneous and inhomogeneous components to the line shape are now well understood [3,4].

In this section we incorporate the above-described Maxwell-Bloch analysis of the field-ion interaction into a detailed collisional-radiative model [24] of the Ne-like germanium ion. We examine specifically the 236-Å transition:

$$(2p^5{}_{1/2}3s)_{J=1}\leftrightarrow(2p^5{}_{1/2}3p_{3/2})_{J=2}$$

(2-1 transition in the following)

and the 196-Å transition:

$$(2p^5{}_{1/2}3s)_{J=1}\leftrightarrow(2p^5{}_{1/2}3p_{1/2})_{J=0}$$

(0-1 transition in the following)

which share a common lower level. We consider two effects relevant to the onset of saturation; first, the coupling of the 196-Å and 236-Å lasing-level populations through stimulated transitions—a relevant issue as much of the recent progress has been in the successful augmentation of the output of the 0-1 transition to intensities comparable with and exceeding those on the 2-1 transitions [25–27] and, second, the possible breakdown of the assumption of a statistical distribution of population among the states of the lasing levels due to the differences in the stimulated transition rates which exist in presence of a linearly propagating field.

Let us label

$$d_2=\langle(2p^5{}_{1/2}3s)_{J=1}\|\vec{d}\|(2p^5{}_{1/2}3p_{3/2})_{J=2}\rangle$$

and

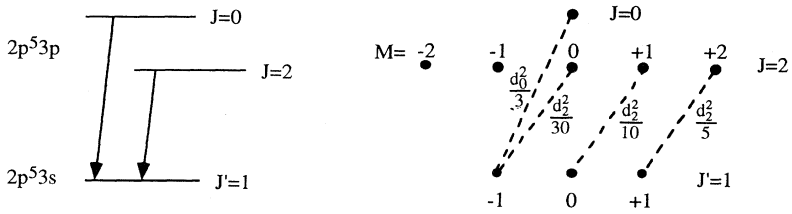

FIG. 3. Values of $\langle JM|d_1|J'M-1\rangle^2=\langle J-M|d_{-1}|J'-M+1\rangle^2$ for the coupled lasing transitions in the Ne-like ion; d_i is the reduced matrix element $\langle J'=1\|\vec{d}\|J=i\rangle$.

$$d_0=\langle(2p^5{}_{1/2}3s)_{J=1}\|\vec{d}\|(2p^5{}_{1/2}3p_{1/2})_{J=0}\rangle .$$

The values of $\langle JM|d_1|J'M-1\rangle^2=\langle J-M|d_{-1}|J'-M+1\rangle^2$ are given in Fig. 3.

The equation system (19) governing the evolution of populations n_{JM} for this case is then

$$\frac{d}{dt}n_{00}=r_{00}-\Gamma_{00}n_{00}-(n_{00}-n_{11})\Gamma_{I(01)} ,$$

$$\frac{d}{dt}n_{2-2}=\frac{d}{dt}n_{22}=r_{22}-\Gamma_{22}n_{22}-(n_{22}-n_{11})\tfrac{3}{2}\Gamma_{I(21)} ,$$

$$\frac{d}{dt}n_{2-1}=\frac{d}{dt}n_{21}=r_{21}-\Gamma_{21}n_{21}-(n_{21}-n_{10})\tfrac{3}{4}\Gamma_{I(21)} ,$$

$$\frac{d}{dt}n_{20}=r_{20}-\Gamma_{20}n_{20}-(n_{20}-n_{11})\tfrac{1}{2}\Gamma_{I(21)} ,$$

$$\frac{d}{dt}n_{1-1}=\frac{d}{dt}n_{11}=r_{11}-\Gamma_{11}n_{11}+(n_{22}-n_{11})\tfrac{3}{2}\Gamma_{I(21)}+(n_{20}-n_{11})\tfrac{1}{4}\Gamma_{I(21)}+(n_{00}-n_{11})\tfrac{1}{2}\Gamma_{I(01)} ,$$

$$\frac{d}{dt}n_{10}=r_{10}-\Gamma_{10}n_{10}+(n_{21}-n_{10})\tfrac{3}{2}\Gamma_{I(21)} ,$$

where

$$\Gamma_{I(JJ')}=\frac{d_J^2 I_{JJ'}(\nu_0,z)}{6\hbar^2\varepsilon_0 c(2J+1)\alpha_{JJ'}} ,$$

i.e.,

$$\Gamma_{I(JJ')}=\frac{B_{JJ'}I_{JJ'}(\nu_0,z)}{c\alpha_{JJ'}} .$$

To perform these calculations we have adapted the collisional-radiative model of Pert [24] which uses a weighted implicit method to solve the matrix equation

$$[q_i^{N+1}-q_i^N]/\Delta t=\sum_{j\neq i}X_{ij}[W_{ij}q_i^{N+1}+(1-W_{ij})q_i^N]-X_{ji}[W_{ji}q_j^{N+1}+(1-W_{ji})q_j^N] ,$$

where q_i^N is the population of level i at the time step N and X_{ij} represents the total rate from level i to level j. In general, the weights W_{ij} are the quasi-analytic positivity preserving forms of

$$W_{ij}=\max\{1/2,1-1/(\max\{N_i,N_j\}\lambda_{ij})\} .$$

Here, N_i is the number of nonzero transition elements connecting i to all other levels and $\lambda_{ij}=(X_{ij}+X_{ji})\Delta t$. The choice of weights is crucial for time-dependent calculations—we leave them for the sake of completeness—but it is largely irrelevant when we allow the system to iterate to a steady state. We note that the apparently simpler method of inverting the rate matrix to obtain steady-state populations is avoided as the matrix is singular for the degenerate states when the contribution of the symmetry breaking stimulated transitions is negligible. The rates X_{ij} contain all significant interlevel terms and with the use of the R-matrix collision rates of Kingston and Robertson [28] have yielded a very satisfactory description of the laser in the small-signal limit [29].

We have developed the model of this earlier work through the separation of the degenerate lasing levels and the inclusion of the stimulated transition rates as discussed in the previous sections. It should be emphasized that, while an asymmetry is introduced into the stimulated emission rates through the absence of π radiation which forbids $\Delta M=0$ transitions, spontaneous emission includes both $\Delta M=\pm1$ and $\Delta M=0$ transitions.

As we have separated some of the levels into their degenerate terms, it is of course necessary to include the elastic collisions which equilibrate the populations of these states in the collisional radiative model. We use the rate coefficient of Delcroix and Bers [15] introduced earlier. Elastic collisions on a state JM with a total rate Γ_e are distributed evenly among the $2J+1$ states JM' of the level J (including $M'=M$ because elastic collisions without change of state are also possible), i.e., the rate of each transition $M-M'$ is $\Gamma_e/(2J+1)$. Similarly, inelastic collision rates $\Gamma_{J'J}$ into a level J are distributed evenly among the $2J+1$ states.

The approach we take is to initially calculate the steady-state populations in the absence of a field and to solve the radiative transfer through a small length of homogeneous plasma—we assume that a 10-mrad segment of the spontaneous emission contributes to the beam, in accordance with typically measured divergences. Only the radiation from the 196-Å and 236-Å transitions are considered. Subsequently, the problem is modeled in a piecewise fashion through the plasma column, each step assuming a constant uniform field for the purpose of solving the atomic populations and amplifying the beam through the plasma thus obtained (appending the appropriate ASE term from the segment).

The populations are calculated in the steady state. While the excited state kinetics can be excellently approximated in this fashion, we note that the ionization relaxation times are generally significantly longer than hydrodynamic time scales. Steady-state calculations thus tend to overestimate the degree of ionization and conse-

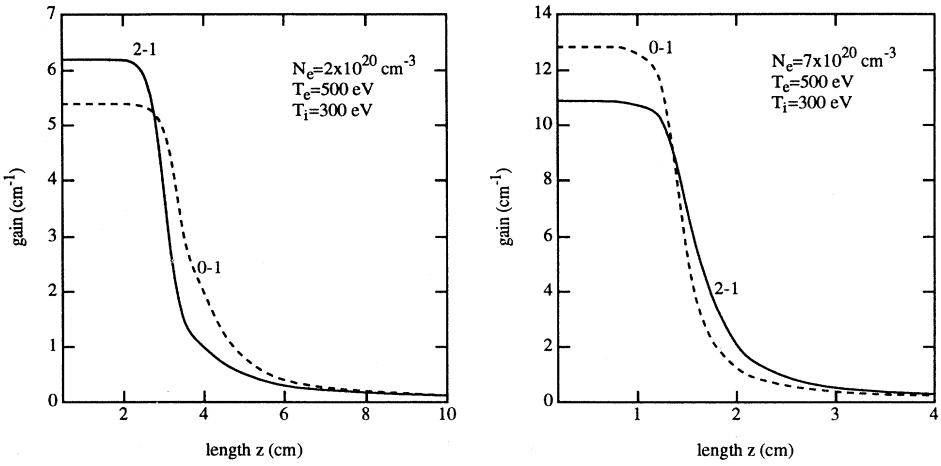

FIG. 4. The gain coefficients as a function of target length for the low- (2×10^{20} cm^{-3}) and high- (7×10^{20} cm^{-3}) density cases, respectively. These gain coefficients are reproduced to within 1% for any assumed value of the elastic collision rate.

quently overestimate pumping due to recombination processes. These are especially significant for gain calculations on the 2-1 lines and we find the gain on these transitions is typically increased by ~20% relative to that on the 0-1 transition.

We use an empirical reduction in the monopole collision excitation rate of the $J=0$ level from the ground level (a driving rate of the 0-1 population inversion) to reproduce experimental observations. This was discussed in detail in earlier work which suggests that a factor of 0.5–0.6 is ideal in germanium. In fact, we use here a value of 0.7 which is preferential for steady-state calculations as it compensates for the recombination effects discussed in the previous paragraph and maintains the correct gain ratio between the 0-1 and 2-1 lines.

We consider two density regimes which are representative of two modes of operation of the laser—the low-density regime sampled in slab target operation and the high-density regime which may be accessed by the use of curved targets or prepulses. We choose electron densities of 2×10^{20} and 7×10^{20} cm^{-3} as being broadly representative. In both cases we assume an electron temperature of 500 eV and an ion temperature of 300 eV.

Initially we consider calculations with an infinite relaxation (elastic collisions) rate between the states—thus accounting for the effects of saturation on the level populations, but neglecting differential effects on the state populations specific to the Maxwell-Bloch treatment.

Figure 4 illustrates the development of the 236-Å and 196-Å gain coefficients as a function of length at the two densities. It is apparent that the 0-1 line is dominant at high density and the 2-1 dominant at low density. The presence of these two regimes is key in describing the different behavior of the slab, curved target and prepulsed experiments [19,30]. In slab targets, the beam can only sample low-density plasma for significant lengths and the 2-1 lines dominate the output. As one enables the beam to sample higher density plasma through the use of either curved targets or prepulses, both the 2-1 and 0-1 lines benefit, but the latter benefits more and dominates the spectrum when the effect is strong enough. We note that large differences in the 2-1 and 0-1 gain coefficients are not required to produce the significant intensity differences measured experimentally. Dependence on elastic collision rates is discussed below.

At both densities the onset of saturation is somewhat later than experimentally observed in slab target operation. In the real laser, the beam follows a refracting path through the lasant, the dense plasma significantly augmenting the source function, but the less dense plasma being the region where saturation tends to occur (as the beam tends to exit in the wings). In the homogeneous plasmas considered here, the dense case provides a reasonable estimation for the source function but overestimates the saturation intensity, whereas the less dense case provides a reasonable value for the saturation intensity but underestimates the source function. In both cases the onset of saturation is thus delayed due to an un-

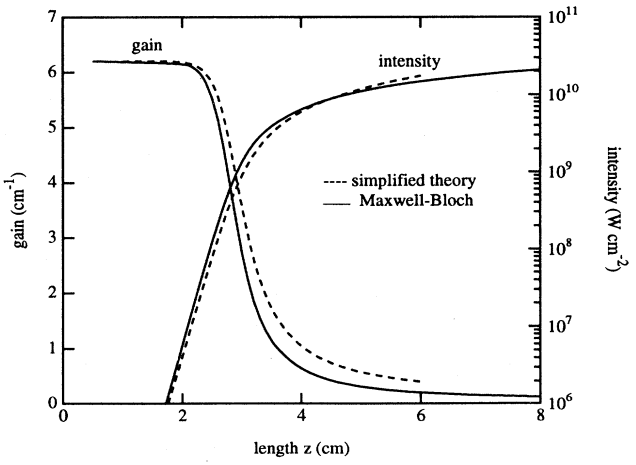

FIG. 5. The gain coefficient and intensity as a function of target length for the 2-1 transition in the low-density (2×10^{20} cm^{-3}) case is given by the Maxwell-Bloch treatment and the simplified theory, respectively. For the simplified theory, gain and intensity values have been taken equal to the Maxwell-Bloch's ones at $z=1$ cm.

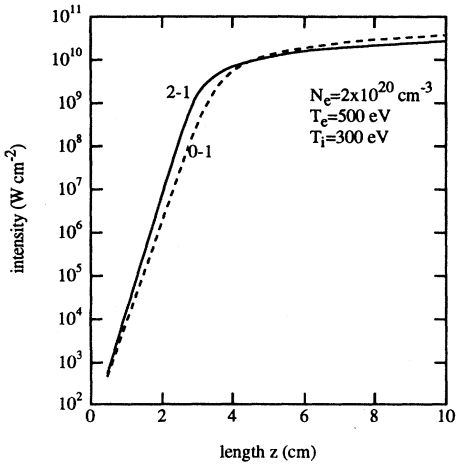

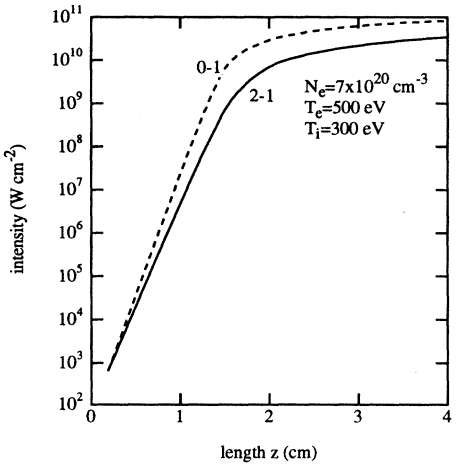

FIG. 6. The intensity scaling as a function of length for the low- (2×10^{20} cm^{-3}) and high- (7×10^{20} cm^{-3}) density cases, respectively. These intensities are reproduced to within 5% for *any* assumed value of the elastic collision rate.

derestimation of the ratio of the source function to the saturation intensity. The model we describe here has, in fact, been coupled with hydrodynamic and raytracing calculation and was found to reproduce the experimentally observed behavior very well [29]. In the present work, for simplicity, we have not considered any effect due to transverse profiles of electron density and gain (see Ref. [5] for a study with Maxwell-Bloch equations, including a fluctuation source term, in a two-level system where degeneracies are not explicitly taken into account). The purpose of this work is primarily to present the detailed Maxwell-Bloch treatment to describe the onset of saturation as the local intensity increases.

It is instructive to compare the results with those of x-ray laser studies using the simple theory of Sec. II. In this, using the small-signal gain coefficient G_0 (gain at line center), the saturation is often analyzed in an approximate way by making use of the saturation intensity $I_S=h\nu/\sigma\tau$ [4,16] (where σ is the cross section for stimulated emission and τ the gain recovery time) and of the simple formula [4,20]

$$G(z)=\frac{I_S}{I(z)+I_S}G_0 ,$$

where the intensity $I(z)=\int d\nu I(\nu,z)\approx\Delta\nu_{\rm amp}I(\nu_0,z)$. Owing to the radiation transfer equation (1′) and to the gain narrowing of the line [$\Delta\nu_{\rm amp}$ is proportional to $(G_0z)^{-1/2}$] we may write

$$I(z+\Delta z)=\left[\frac{z}{z+\Delta z}\right]^{1/2}e^{G(z)\Delta z}I(z) .$$

In Fig. 5 we show the comparison between the results obtained in using these two coupled equations, and the results presented in Fig. 4 and Fig. 6, for the 2-1 transition and the low-density case. Differences appear clearly at saturation, where the Maxwell-Bloch treatment is more rigorous. For instance, at $z=3$ cm, the intensity is 1.4×10^9 W cm^{-2} (Maxwell-Bloch) against 9×10^8 W cm^{-2} (simplified theory, 36% smaller), and the local gain is 2.7 cm^{-1} (Maxwell-Bloch) against 3.6 cm^{-1} (simplified theory, 33% larger).

In Fig. 6, we note the relatively obvious point that the saturation intensity is approximately proportional to the electron density (through the collision rates) and thus that lasing systems which facilitate beam propagation through high density plasma will benefit from a higher saturation intensity. These points are clarified in Fig. 6

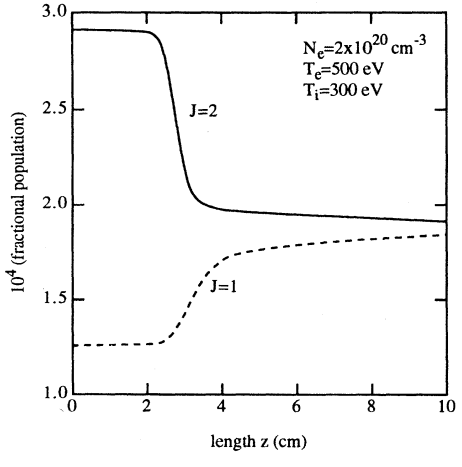

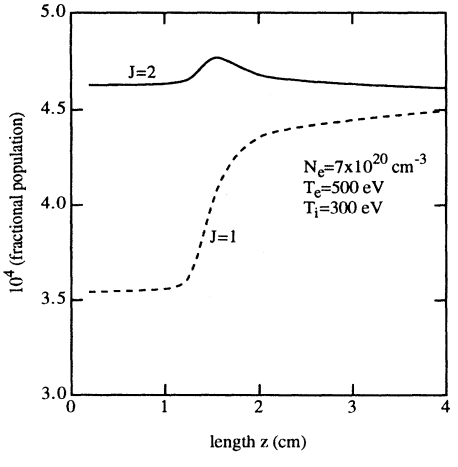

FIG. 7. The steady state $J=2$ and $J=1$ level populations per unit statistical weight as a function of plasma length for a calculation which assumes an infinite relaxation (elastic collisions) rate among the states which comprise the levels. The two graphs represent the low- (2×10^{20} cm^{-3}) and high- (7×10^{20} cm^{-3}) density cases, respectively.

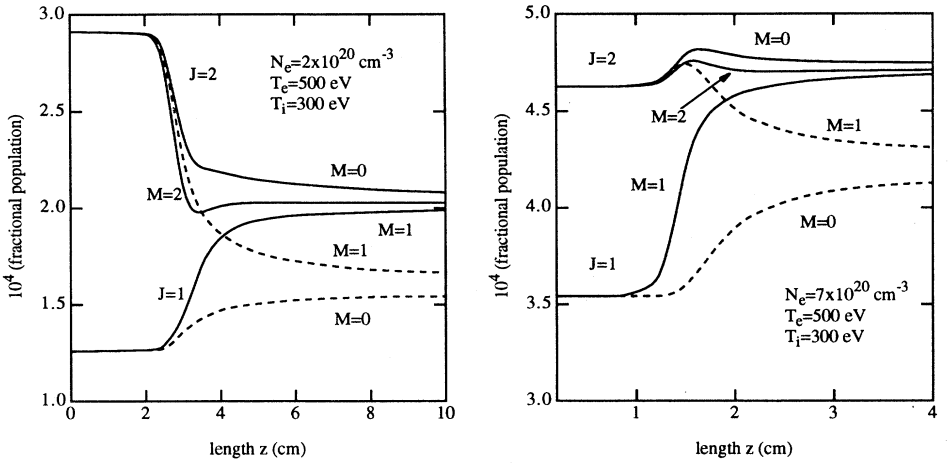

FIG. 8. The steady state $J=2$ and $J=1$ state populations as a function of plasma length for a calculation which assumes a zero relaxation (elastic collisions) rate among the states which comprise the levels. The two graphs represent the low-(2×10^{20} cm^{-3}) and high-(7×10^{20} cm^{-3}) density cases, respectively. Individual state populations vary markedly from the "averaged" populations in the previous figure.

which plots the variation of intensity with plasma length for the two densities. The dependence on the elastic collision rate is discussed below.

Figure 7 illustrates the development of the state populations of the 2-1 transition as a function of length for the case of an infinite elastic collision rate. In the low-density case, the 2-1 line dominates the lasing and hence the saturation behavior. The populations obey the expected saturation behavior, tending to a weighted average of the unperturbed populations. In the high density case, the behavior is significantly different. The 0-1 line is the first to saturate and the $J=2$ population is at first driven upwards as a consequence of this, before the 2-1 line saturates also.

Figure 8 illustrates the identical case when the elastic rates are set to zero, thus enabling the effect on the states to be clearly seen. At the onset of saturation, the populations of the five states (represented as three through the symmetry in $\pm M$) of the $J=2$ level separate as a consequence of the asymmetry in the stimulated emission rates imposed by the absence of π polarized radiation, the $M=\pm2$ populations falling most rapidly as these states interact only with $\sigma\pm$ radiation in any case. A small distance beyond the onset of 2-1 saturation, the 0-1 line itself begins to saturate and stimulated emission on this transition begins to affect populations. The result is a surge in population of $J=1, M=\pm1$ states which are the lower states of the 0-1 lasing line, accompanied by a second-order effect in the $J=2, M=0, \pm2$ states which are coupled to these states. In the high-density case, the different behavior arises as a consequence of the 0-1 transition dominating the lasing and being responsible for the saturation behavior. The initial effect is a rapid increase in the population of $J=1, M=\pm1$ states (through pumping from the $J=0$ level), with consequent effects on the connected $J=2, M=0, \pm2$ states as the 236-Å radiation density nears saturation values.

Figure 9 illustrates the effect on the redistribution of the level populations through elastic collisions. The elastic collisions are fast enough to ensure almost complete redistribution of the $J=2$ level, while discrepancies of the order of 1 to a few percent (according to the density) remain in the $J=1$ states—an effect which can surely be neglected. Circumstances can be envisaged in which the effects are significant—a beam saturated in high-density plasma passing through low-density plasma, for

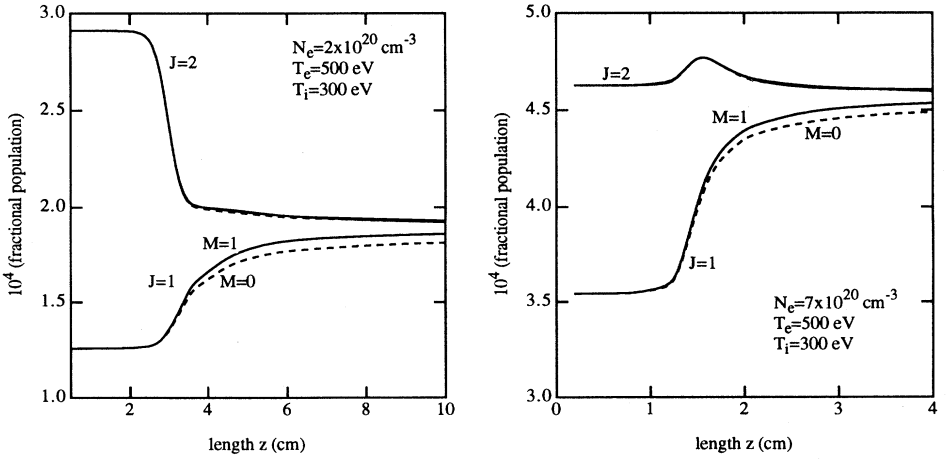

FIG. 9. The steady state $J=2$ and $J=1$ states populations as a function of plasma length for a calculation which assumes an analytic form (Ref. [15]) for the elastic collision rate which redistributes the population among the states which comprise the levels. The two graphs represent the low- (2×10^{20} cm^{-3}) and high-(7×10^{20} cm^{-3}) density cases, respectively.

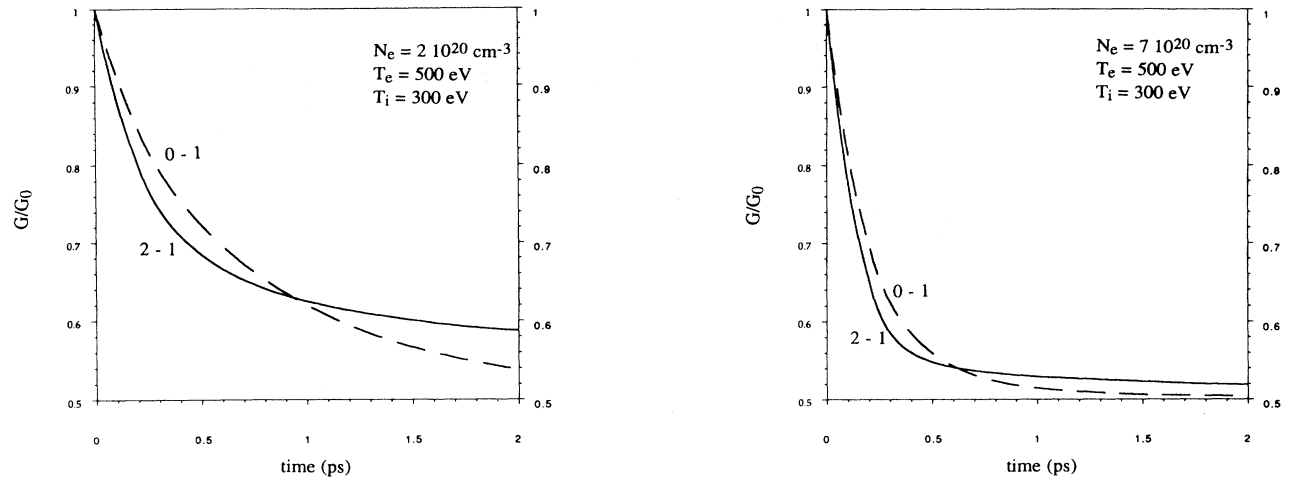

FIG. 10. Temporal evolution of gain in the plasma slice that radiation reaches at time $t=0$ with an intensity I close to the saturation intensity I_S [$I \approx I_S = (h\nu/\sigma\tau)$]. The curves correspond to $I = 1.8\times10^9$ W/cm^2 (0-1 line) and $I = 1.2\times10^9$ W/cm^2 (2-1 line) with an electron density of 2×10^{20} cm^{-3}, and $I = 4.8\times10^9$ W/cm^2 (0-1 line) and $I = 2.9\times10^9$ W/cm^2 (2-1 line) with electron density 7×10^{20} cm^{-3}. G_0 is the corresponding small-signal gain.

instance—but in simple cases it appears unlikely that these are of practical relevance. It must however be pointed out that the elastic-collision rates that we have used are approximate. Even if the main features here obtained are likely not questionable, more accurate estimations of elastic-collision rates for the different states involved should be useful.

In contrast to the individual M-state populations, the gain and intensity evolutions are found to be weakly dependent on the elastic collision rate, as mentioned in Fig. 4 and Fig. 6. This may result in part from the approximation used in this work (that the total rate is distributed evenly among the states, in particular). But we must first notice that the gain is proportional to a sum of products $(n_{JM}-n_{J'M-1})\langle JM|d_1|J'M-1\rangle^2$ [see Eq. (16)]. So, pertinent comparisons must relate to population differences $(n_{JM}-n_{J'M-1})$ rather than to populations n_{JM} themselves. One can see in comparing Fig. 7 and Fig. 8 that the population differences $(n_{JM}-n_{J'M-1})$ are much less sensitive to the elastic-collision rate than the populations themselves. Moreover, in the problem considered here, where the lower level is involved in two lasing lines, a number of elementary processes—radiative (absorption and stimulated emission) and collisional transitions—are coupled and the analysis cannot be achieved by considering either of them alone.

In Fig. 10 we show the characteristic temporal evolution of local gain in a plasma slice just at the beginning of the x-ray laser pulse, in a region where the incoming intensity (at local time $t=0$) is already large enough to produce saturation. As an example, this slice is close to $z=3$ cm for the 2-1 radiation in the low density case (see Fig. 4). Results are obtained using the time-dependent solutions of equation system (19), the initial population densities being the steady-state values calculated with intensity equal to zero (they correspond to the small-signal gain G_0). In presence of radiation, the steady regime is reached in a time of the order of 0.5 to 2 ps, according to the plasma density.

The equations, and the corresponding quantitative results here obtained, have been derived using the assumption that the values of coherence envelopes $\hat{\rho}_{J'M-1,JM}$ correspond to quasi-steady-state (QSS) with respect to their production and decay processes. Since

$$\frac{d}{dt}\hat{\rho}_{J'M-1,JM} = -(\Gamma + i\delta_L)\hat{\rho}_{J'M-1,JM} + \frac{i\tilde{E}}{\hbar}\langle JM|d_1|J'M-1\rangle \times (n_{JM}-n_{J'M-1}) ,$$

this assumption is valid provided that the populations do not vary significantly during the time interval Γ^{-1}. This is clearly true below saturation. When the radiation intensity is large, the characteristic time of evolution of population densities is Γ_I^{-1} with $\Gamma_{I(JJ')} = \{[B_{JJ'}I_{JJ'}(\nu_0,z)]/(c\alpha_{JJ'})\}$ where $\alpha = (\Delta\nu/\Delta\nu_{\text{amp}})$ (see above). The time Γ_I^{-1} is long compared with Γ^{-1} if $\Gamma_I \ll \Gamma$. Considering the cross section for stimulated emission [31] $\sigma = (G_0/g_u\Delta n_{ul}) \approx (h\nu B/\Delta\nu c)$, and the total intensity $I = \int d\nu I(\nu) \approx \Delta\nu_{\text{amp}} I(\nu_0)$, it comes $\Gamma_I \approx (\sigma I/h\nu)$ or $I \approx (h\nu/\sigma)\Gamma_I$.

In the high-density case (7×10^{20} cm^{-3}), $\Gamma = 2.8\times10^{13}$ s^{-1}. So, with $\Gamma_I \le 2.8\times10^{12}$ s^{-1}, the condition is $I \le 2.9\times10^{10}$ W/cm^2 for the 0-1 line (obtained at $z \approx 2$ cm), a value six times greater than the "saturation intensity" [$(h\nu/\sigma\tau)$, [4,16]] $I_S \approx 4.8\times10^9$ W/cm^2 (obtained at $z \approx 1.5$ cm), and $I \le 2.1\times10^{10}$ W/cm^2 for the 2-1 line (obtained at $z \approx 2.8$ cm) while $I_S \approx 2.9\times10^9$ W/cm^2 (obtained at $z \approx 1.6$ cm).

In the low-density case (2×10^{20} cm^{-3}), $\Gamma = 9\times10^{12}$ s^{-1}. This leads to $I \le 9.3\times10^9$ W/cm^2 for the 0-1 line (obtained at $z \approx 4.5$ cm) while $I_S \approx 1.8\times10^9$ W/cm^2 (ob-

tained at $z \approx 3.3$ cm), and $I \leq 6.9 \times 10^9$ W/cm^2 for the 2-1 line (obtained at $z \approx 4.5$ cm) while $I_S \approx 1.2 \times 10^9$ W/cm^2 (obtained at $z \approx 3$ cm). So, in all cases, the method is suited to describe the plasma and radiation evolution until intensities far above the "saturation intensity" (a factor of 5 in intensity for the least favorable case).

IX. CONCLUSION

This work gives a general theoretical description of populations and radiation intensities coupled evolutions suitable for plasma samples exhibiting population inversions between levels connected by electric-dipole transitions. The equations are valid whatever the radiation intensities are, provided that the coherence envelopes may be assumed in steady state relative to their production and decay processes. For the Ne-like Ge^{22+} ion considered in detail in this work, by way of illustration, this is verified for intensities up to five times (at least) the saturation intensity.

At low intensities the solutions correspond to the usual ASE regime (below saturation) with a constant gain value along the z axis. This gain value is consistent with the Einstein coefficient for stimulated emission as calculated by the Fermi golden rule.

At high intensities approaching saturation it is no longer valid to consider a level as a whole interacting with the radiation. The specific individual-state interactions must be taken into account, as shown in this work.

The present theory is appropriate to describe the gradual transition to saturation of x-ray lasers in plasmas when the ASE intensities become large. It must be pointed out that the elastic-collision rates are important parameters, as well for spectral line profiles as for saturation behavior. Even if reasonable estimates of these parameters are provided by an available approximate formula, accurate elastic-collision rates for different involved states should be useful.

For the Ne-like Ge^{22+} ion, we find that the equal population redistribution of the states of one level by elastic collisions is almost complete, despite the fact that the interactions with the radiation are not equal between the different states. Thus, although our results have arisen from the use of an approximate elastic-collision rate and may not be valid for the general case, one may ask whether the simple theory of Sec. II (which considers a level as a whole and ignores the individual M states) is sufficient to study the transition to saturation. The important point is that the Maxwell-Bloch treatment is undoubtedly more rigorous in obtaining the correct quantitative population evolution. The fact that the individual M population differences are small due to collisional redistribution is another point. When saturation occurs, the equations for populations and for gain are not strictly rigorous in the simple theory of Sec. II, which ignores the individual M states and their specific interactions to a given radiation. The results converge only if the rates of collisional transitions $JM - JM'$ are large enough to ensure the equalization of states' populations pertaining to a common level, whatever the radiation intensity is. This key point is only assumed, not verified in the simple theory. In contrast, the theory presented in this paper does not need such an assumption, and gives the correct result in any case, whether the statistical redistribution of population occurs or not. Nevertheless we would expect the use of the simple theory to be adequate for most practical applications.

ACKNOWLEDGMENTS

We are grateful to G. J. Pert for providing the collisional radiative model which we have adapted for these purposes. Additionally, we thank A. E. Kingston and E. Robertson for providing the collision excitation rates and for useful discussions.

APPENDIX

The polarization vector

The polarization vector $\vec{P}$ is given by

$$\vec{P} = \mathrm{Tr}(\rho \vec{d}) ,$$

i.e.,

$$\vec{P} = \mathrm{Tr}\left[\rho \sum_{J'M'} |J'M'\rangle\langle J'M'|\vec{d}\right] ,$$

or

$$\vec{P} = \sum_{JMJ'M'} \langle JM|\rho|J'M'\rangle\langle J'M'|\vec{d}|JM\rangle ,$$

where ρ is the density operator and $\vec{d}$ is the atomic electric dipole.

We shall use the notation $\rho_{JM,J'M'} = \langle JM|\rho|J'M'\rangle$. Considering one particular dipolar transition with upper level J and lower level J', and using $\vec{d} = \sum_q d_q \vec{e}_q$, leads to

$$\vec{P} = \sum_{Mq} [\langle J'M+q|d_q|JM\rangle \rho_{JM,J'M+q} + \langle JM+q|d_q|J'M\rangle \rho_{J'M,JM+q}]\vec{e}_q ,$$

or

$$\vec{P} = \sum_{Mq} [\langle J'M+q|d_q|JM\rangle \rho_{JM,J'M+q} + \langle JM|d_q|J'M-q\rangle \rho_{J'M-q,JM}]\vec{e}_q .$$

Matrix elements such as $\langle J'M+q|d_q|JM\rangle$ are real numbers which verify

$$\langle J'M+q|d_q|JM\rangle = (-1)^q \langle JM|d_{-q}|J'M+q\rangle$$

so that we may also write

$$\vec{P}=\sum_q \sum_M [\langle JM|d_q|J'M-q\rangle\rho_{J'M-q,JM}+(-1)^q\langle JM|d_{-q}|J'M+q\rangle\rho_{JM,J'M+q}]\vec{e}_q$$

[Eq. (7) in Sec. III].

Considering one particular dipolar transition connecting levels J and J', the atomic electric dipole is

$$\vec{d}=\sum_{MM'}\vec{d}_{J'M',JM}|J'M'\rangle\langle JM|+\sum_{MM'}\vec{d}_{JM,J'M'}|JM\rangle\langle J'M'|$$
$$=\sum_{Mq}\langle J'M+q|d_q|JM\rangle\vec{e}_q|J'M+q\rangle\langle JM|+\sum_{Mq}\langle JM|d_q|J'M-q\rangle\vec{e}_q|JM\rangle\langle J'M-q| \ .$$

As

$$\langle JM|d_q|J'M-q\rangle=(-1)^q\langle J'M-q|d_{-q}|JM\rangle$$

the last term of the above equation is also $\sum_{Mq}(-1)^q\langle J'M-q|d_{-q}|JM\rangle\vec{e}_q|JM\rangle\langle J'M-q|$ or, equivalently, $\sum_{Mq}(-1)^q\langle J'M+q|d_q|JM\rangle\vec{e}_{-q}|JM\rangle\langle J'M+q|$, and hence

$$\vec{d}=\sum_{Mq}\langle J'M+q|d_q|JM\rangle[|J'M+q\rangle\langle JM|\vec{e}_q+(-1)^q|JM\rangle\langle J'M+q|\vec{e}_{-q}]$$

(the fact that $\vec{d}$ is real appears clearly in this expression). Accordingly, the product $\vec{d}\cdot\vec{E}$ may be written as

$$\vec{d}\cdot\vec{E}=\sum_{Mq}\langle J'M+q|d_q|JM\rangle[|JM\rangle\langle J'M+q|E_q+(-1)^q|J'M+q\rangle\langle JM|E_{-q}] \ .$$

This last expression is convenient for using in Eq. (8), Sec. III. So, with the $\sigma+$ field given by Eq. (5) of Sec. III, Eq. (8) and approximation (1) of Sec. IV give in particular

$$\frac{d}{dt}\rho_{J'M,JM}=i\omega_A\rho_{J'M,JM}$$
$$+\frac{i\tilde{E}}{\hbar}(\langle JM+1|d_1|J'M\rangle\rho_{JM+1,JM}-\langle JM|d_1|J'M-1\rangle\rho_{J'M,J'M-1})e^{i(\omega t-kz+\varphi_+)} \ ,$$

$$\frac{d}{dt}\rho_{J'M-1,JM}=i\omega_A\rho_{J'M-1,JM}$$
$$+\frac{i\tilde{E}}{\hbar}\langle JM|d_1|J'M-1\rangle(\rho_{JM,JM}-\rho_{J'M-1,J'M-1})e^{i(\omega t-kz+\varphi_+)} \ ,$$

$$\frac{d}{dt}\rho_{JM,J'M+1}=-i\omega_A\rho_{JM,J'M+1}$$
$$+\frac{i\tilde{E}}{\hbar}(\langle JM|d_1|J'M-1\rangle\rho_{J'M-1,J'M+1}-\langle JM+2|d_1|J'M+1\rangle\rho_{JM,JM+2})e^{-i(\omega t-kz+\varphi_+)} \ .$$

As the coherences are initially equal to zero, and the populations different from zero, only coherences $\rho_{J'M-1,JM}$ can become nonzero at later times. The slower evolution of (Zeeman) coherences of the type $\rho_{JM,JM'}$ or $\rho_{J'M,J'M'}$ with $M\neq M'$ are of second order and will be neglected. So, defining

$$\hat{\rho}_{J'M-1,JM}=\rho_{J'M-1,JM}e^{-i(\omega t-kz+\varphi_+)}$$

and

$$\delta_L=\omega-\omega_A \ ,$$

we obtain (neglecting $\partial\varphi_+/\partial t$ with respect to ω, consistently with the paraxial approximation):

$$\frac{d}{dt}\hat{\rho}_{J'M-1,JM}=-i\delta_L\hat{\rho}_{J'M-1,JM}+\frac{i\tilde{E}}{\hbar}\langle JM|d_1|J'M-1\rangle(n_{JM}-n_{J'M-1})$$

to which should be added the collisional total decay of the coherence (including by elastic electron-ion collisions), the rate of which is labeled Γ, to obtain finally

$$\frac{d}{dt}\hat{\rho}_{J'M-1,JM}=-(\Gamma+i\delta_L)\hat{\rho}_{J'M-1,JM}+\frac{i\tilde{E}}{\hbar}\langle JM|d_1|J'M-1\rangle(n_{JM}-n_{J'M-1}) \ .$$

The approximation (2) of Sec. IV $[(d/dt)\hat{\rho}_{J'M-1,JM}=0]$ then leads to

$$\hat{\rho}_{J'M-1,JM}=\frac{i\tilde{E}}{\hbar}\langle JM|d_1|J'M-1\rangle(n_{JM}-n_{J'M-1})\frac{\Gamma-i\delta_L}{\delta_L^2+\Gamma^2}$$

where d_1 is the standard tensorial component of $\vec{d}$ on $\vec{e}_1$, namely,

$$d_1=-\frac{1}{\sqrt{2}}(d_x+id_y)\ .$$

Let us define $\Psi(\omega)$ by the relation

$$\frac{\Gamma-i\delta_L}{\delta_L^2+\Gamma^2}=\pi\Psi(\omega)\ .$$

Equation (7) in Sec. III leads now to

$$\vec{P}_{\sigma+}=\sum_M\langle JM|d_1|J'M-1\rangle^2(n_{JM}-n_{J'M-1})\frac{i\pi\tilde{E}}{\hbar}[e^{i(\omega t-kz+\varphi_+)}\Psi(\omega)\vec{e}_1+e^{-i(\omega t-kz+\varphi_+)}\Psi^*(\omega)\vec{e}_{-1}]$$

i.e.,

$$\vec{P}_{\sigma+}=\frac{i\pi}{\hbar}\Psi(\omega)\sum_M\langle JM|d_1|J'M-1\rangle^2(n_{JM}-n_{J'M-1})\tilde{E}e^{i(\omega t-kz+\varphi_+)}\vec{e}_1+\text{H.c.}$$

[Eq. (10), Sec. IV].

In a quite similar way, with the σ_- field given by Eq. (6) of Sec. III we obtain

$$\vec{P}_{\sigma-}=\frac{i\pi}{\hbar}\Psi^*(\omega)\sum_M\langle JM|d_{-1}|J'M+1\rangle^2(n_{JM}-n_{J'M+1})\tilde{E}e^{-i(\omega t-kz+\varphi_-)}\vec{e}_1+\text{H.c.}$$

[Eq. (11), Sec. IV].

Wave equation

By considering the Wigner-Eckart theorem and the 3-j symbol properties it can be readily shown that

$$\langle JM|d_{-1}|J'M+1\rangle=(-1)^{J'-J+1}\langle J-M|d_1|J'-M-1\rangle\ .$$

Therefore, whenever the symmetry $M\leftrightarrow(-M)$ is statistically preserved by the physical processes, $n_{JM}=n_{J-M}, n_{J'M+1}=n_{J'-M-1}$, etc., and hence

$$\langle JM|d_{-1}|J'M+1\rangle^2(n_{JM}-n_{J'M+1})=\langle J-M|d_1|J'-M-1\rangle^2(n_{J-M}-n_{J'-M-1})\ .$$

Summing over $M(-J\le M\le J)$ is equivalent to summing over $M'=-M(-J\le M'\le J)$, so

$$\sum_M\langle JM|d_{-1}|J'M+1\rangle^2(n_{JM}-n_{J'M+1})=\sum_{M'}\langle JM'|d_1|J'M'-1\rangle^2(n_{JM'}-n_{J'M'-1})\ .$$

On the rhs, the dummy index M' can be relabeled M, which proves that

$$\sum_M\langle JM|d_{-1}|J'M+1\rangle^2(n_{JM}-n_{J'M+1})=\sum_M\langle JM|d_1|J'M-1\rangle^2(n_{JM}-n_{J'M-1})\ .$$

Let us call $U_{JJ'}$ this common value. Then, reporting $\vec{E}_{\sigma+}$ [Eq. (5)] and $\vec{P}_{\sigma+}$ [Eq. (10)] in Eq. (4) gives

$$\left[\vec{\nabla}^2-\frac{1}{c^2}\frac{\partial^2}{\partial t^2}-\frac{\omega_{pe}^2}{c^2}\right]\tilde{E}e^{i(\omega t-kz+\varphi_+)}\vec{e}_1+\text{H.c.}=\frac{1}{\varepsilon_0c^2}\frac{\partial^2}{\partial t^2}\frac{i\pi}{\hbar}\Psi(\omega)U_{JJ'}\tilde{E}e^{i(\omega t-kz+\varphi_+)}\vec{e}_1+\text{H.c.}$$

Projection on $\vec{e}_1$ gives

$$\left[\vec{\nabla}^2-\frac{1}{c^2}\frac{\partial^2}{\partial t^2}-\frac{\omega_{pe}^2}{c^2}\right]\tilde{E}e^{i(\omega t-kz+\varphi_+)}=\frac{1}{\varepsilon_0c^2}\frac{\partial^2}{\partial t^2}\frac{i\pi}{\hbar}\Psi(\omega)U_{JJ'}\tilde{E}e^{i(\omega t-kz+\varphi_+)}\ .$$

Similarly, reporting $\vec{E}_{\sigma-}$ [Eq. (6)] and $\vec{P}_{\sigma-}$ [Eq. (11)] in Eq. (4) leads to

$$\left[\vec{\nabla}^2-\frac{1}{c^2}\frac{\partial^2}{\partial t^2}-\frac{\omega_{pe}^2}{c^2}\right]\tilde{E}e^{-i(\omega t-kz+\varphi_-)}=-\frac{1}{\varepsilon_0c^2}\frac{\partial^2}{\partial t^2}\frac{i\pi}{\hbar}\Psi^*(\omega)U_{JJ'}\tilde{E}e^{-i(\omega t-kz+\varphi_-)}$$

which, apart from φ_- in place of φ_+, is the complex conjugate of the previous equation. Now, if the field propagating along the z axis is correctly described by (5) and (6), the condition $\vec{\nabla}\cdot\vec{E}=0$ leads to[2]

$$\vec{\nabla}_\perp^2\tilde{E}e^{i(\omega t-kz+\varphi)}=0 .$$

Using finally the usual paraxial approximation (see, for example, Ref. [5]), and the retarded time variable $t-z/c$, Eq. (4) becomes

$$\left[\frac{\partial\varphi}{\partial z}-\frac{\omega_{pe}^2}{2kc^2}\right]\tilde{E}-i\frac{\partial\tilde{E}}{\partial z}=-\frac{ikU_{JJ'}}{2\varepsilon_0\hbar}\pi\Psi(\omega)\tilde{E} ,$$

for $\sigma+$

$$\left[\frac{\partial\varphi}{\partial z}-\frac{\omega_{pe}^2}{2kc^2}\right]\tilde{E}+i\frac{\partial\tilde{E}}{\partial z}=\frac{ikU_{JJ'}}{2\varepsilon_0\hbar}\pi\Psi^*(\omega)\tilde{E}$$

for $\sigma-$.

---

[2]With the σ_+ field in Cartesian coordinates, the condition reads as $[(\partial E/\partial x)+E(\partial\varphi/\partial y)]\cos(\omega t-kz+\varphi)+[(\partial E/\partial y)-E(\partial\varphi/\partial x)]\sin(\omega t-kz+\varphi)=0$ for all t, i.e., $(\partial\tilde{E}/\partial x)=-\tilde{E}(\partial\varphi/\partial y)$ and $(\partial\tilde{E}/\partial y)=\tilde{E}(\partial\varphi/\partial x)$. Consequently $(\vec{\nabla}_\perp\tilde{E})^2=\tilde{E}^2(\vec{\nabla}_\perp\varphi)^2$, $\vec{\nabla}_\perp\tilde{E}\cdot\vec{\nabla}_\perp\varphi=0$, $\vec{\nabla}_\perp^2\tilde{E}=\tilde{E}(\vec{\nabla}_\perp\varphi)^2=(1/\tilde{E})(\vec{\nabla}_\perp\tilde{E})^2$, and $\vec{\nabla}_\perp^2\tilde{E}e^{i(\omega t-kz+\varphi)}=[\vec{\nabla}_\perp^2\tilde{E}-(1/\tilde{E})(\vec{\nabla}_\perp\tilde{E})^2]e^{i(\omega t-kz+\varphi)}=0$. The same holds for the $\sigma-$ field.

---

[1] For a recent review see papers in *X-Ray Lasers 1992, Proceedings of the 3rd International Colloquium on X-ray Lasers,* edited by E. E. Fill, IOP Conf. Ser. No. 125 (Institute of Physics, Bristol, 1992) and in *X-Ray Lasers 1994, Proceedings of the Fourth International Colloquium on X-ray Lasers,* edited by D. C. Eder and D. L. Matthews, AIP Conf. Proc. No. 332 (American Institute of Physics, New York, 1994).

[2] A. E. Siegman, *Lasers* (University Science Books, Mill Valley, CA, 1986).

[3] J. A. Koch, B. J. MacGowan, L. B. DaSilva, D. L. Matthews, J. H. Underwood, B. J. Batson, and S. Mrowka, Phys. Rev. Lett. **68**, 3291 (1992).

[4] G. J. Pert, J. Opt. Soc. Am. B **11**, 1425 (1994).

[5] M. Strauss, Phys. Fluids B **1**, 907 (1989).

[6] G. Hazak and A. Bar-Shalom, Phys. Rev. A **38**, 1300 (1988).

[7] R. A. London, M. Strauss, and M. D. Rosen, Phys. Rev. Lett. **65**, 563 (1990).

[8] P. Amendt, R. A. London, and M. Strauss, Phys. Rev. A **44**, 7478 (1991).

[9] E. A. Watson, H. M. Gibbs, F. P. Mattar, M. Cormier, Y. Claude, S. L. McCall, and M. S. Feld, Phys. Rev. A **27**, 1427 (1983); see also, F. P. Mattar and C. M. Bowden, *ibid.* **27**, 345 (1983); D. Polder, M. F. H. Schuurmans, and Q. H. F. Vrehen, *ibid.* **19**, 1192 (1979); E. Ressayre and A. Tallet, *ibid.* **15**, 2410 (1977).

[10] A. Crubellier, S. Liberman, and P. Pillet, J. Phys. B **19**, 2959 (1986); see also, A. Crubellier, Phys. Rev. A **15**, 2430 (1977); J. Phys. (Paris) **47**, C6-211 (1986); M. Gross, *ibid.* **47**, C6-223 (1986).

[11] A. Sureau, in *X-Ray Lasers 1992* (Ref. [1]), p. 251. See also Laser Part. Beams **10**, 787 (1992); A. Sureau and B. Rus (unpublished).

[12] A. P. Yutsis, I. B. Levinson, and V. V. Vanagas, *Mathematical Apparatus of the Theory of Angular Momentum,* Israel Program for Scientific Translations, Jerusalem, 1962), translated from Russian.

[13] B. R. Judd, *Operator Techniques in Atomic Spectroscopy* (McGraw-Hill, New York, 1963).

[14] See A. Crubellier or M. Gross, J. Phys. (Paris) **47**, C6-211 (1986); **47**, C6-223 (1986).

[15] J. L. Delcroix and A. Bers, *Physique des Plasmas* (InterÉditions/CNRS Éditions, Paris, 1994), tome 2, p. 352.

[16] A. Carillon, H. Z. Chen, P. Dhez, L. Dwivedi, J. Jacoby, P. Jaeglé, G. Jamelot, Jie Zhang, M. H. Key, A. Kidd, A. Klisnick, R. Kodama, J. Krishnan, C. L. S. Lewis, D. Neely, P. Norreys, D. O'Neill, G. J. Pert, S. A. Ramsden, J. P. Raucourt, G. J. Tallents, and J. Uhomoibhi, Phys. Rev. Lett. **68**, 2917 (1992).

[17] B. J. MacGowan, L. B. Da Silva, D. J. Fields, C. J. Keane, J. A. Koch, R. A. London, D. L. Matthews, S. Maxon, S. Mrowka, A. L. Oserheld, J. H. Scofield, G. Shimkaveg, J. E. Trebes, and R. S. Walling, Phys. Fluids B **4**, 2326 (1992).

[18] A. Dulieu and S. Jacquemot, in *X-Ray Lasers 1992* (Ref. [1]), p. 239.

[19] J. A. Plowes, S. B. Healy, G. J. Pert, and D. Toft (unpublished).

[20] M. D. Feit and J. A. Fleck, J. Opt. Soc. Am. B **7**, 2048 (1990).

[21] R. A. London, M. D. Rosen, M. S. Maxon, D. C. Eder, and P. L. Hagelstein, J. Phys. B **22**, 3363 (1989).

[22] R. P. Rathowsky, R. S. Craxton, M. D. Feit, R. A. London, R. W. Wallings, G. M. Shimkaveg, A. L. Osterheld, and M. R. Carter, in *X-Ray Lasers 1992* (Ref. [1]), p. 315.

[23] R. P. Rathowsky, R. A. London, R. S. Craxton, M. D.

Feit, R. W. Wallings, and G. M. Shimkaveg, SPIE Proc. **2012**, 41 (1994).
[24] G. J. Pert, J. Comput. Phys. **39**, 251 (1980).
[25] G. F. Cairns, M. J. Lamb, C. L. S. Lewis, A. G. MacPhee, D. Neely, P. Norreys, M. H. Key, C. Smith, S. B. Healy, P. B. Holden, G. Pert, and J. A. Plowers, in *X-Ray Lasers 1994* (Ref. [1]), p. 289.
[26] J. Nilsen, J. C. Moreno, J. A. Koch, J. H. Scofield, B. J. MacGowan, and L. B. Da Silva in *X-Ray Lasers 1994* (Ref. [1]), p. 271.
[27] B. Rus, A. Carillon, B. Gauthé, P. Goedtkindt, P. Jaeglé, G. Jamelot, A. Klisnick, A. Sureau, and P. Zeitoun, J. Opt. Soc. Am. B **11**, 564 (1994).
[28] A. E. Kingston and E. Roberston (private communication).
[29] P. B. Holden, S. B. Healy, M. T. M. Lightbody, G. J. Pert, J. A. Plowes, A. E. Kingston, E. Robertson, C. L. S. Lewis, and D. Neely, J. Phys. B **27**, 341 (1994).
[30] J. A. Plowes, G. J. Pert, and P. Holden (unpublished).
[31] R. C. Elton, *X-Ray Lasers* (Academic, San Diego, 1990).